Theoretical Insights into the Structures of Graphene Oxide and Its Chemical Conversions Between Graphene

6 AUTHORS, INCLUDING:

Xingfa Gao
Chinese Academy of Sciences
64 PUBLICATIONS **895** CITATIONS

SEE PROFILE

Yuliang Zhao
Chinese Academy of Sciences
325 PUBLICATIONS **8,471** CITATIONS

SEE PROFILE

Zhongfang Chen
University of Puerto Rico at Rio Piedras
200 PUBLICATIONS **5,415** CITATIONS

SEE PROFILE

Theoretical Insights Into the Structures of Graphene Oxide and Its Chemical Conversions Between Graphene

Xingfa Gao[1], De-en Jiang[2], Yuliang Zhao[3, 4], Shigeru Nagase[5],
Shengbai Zhang[1], and Zhongfang Chen[6, *]

[1] *Department of Physics, Applied Physics and Astronomy, Rensselaer Polytechnic Institute, Troy, New York 12180, USA*
[2] *Chemical Sciences Division, Oak Ridge National Laboratory, MS6201, Oak Ridge, Tennessee 37931-6201, USA*
[3] *Key Laboratory for Biomedical Effects of Nanomaterials and Nanosafety, Institute of High Energy Physics,*
Chinese Academy of Sciences, Beijing 100049, People's Republic of China
[4] *National Center for Nanoscience and Technology of China, Beijing 100080, People's Republic of China*
[5] *Institute for Molecular Science, Department of Theoretical and Computational Molecular Science, Myodaiji, Okazaki 444-8585, Japan*
[6] *Institute of Functional Nanomaterials, Department of Chemistry, University of Puerto Rico, San Juan, Puerto Rico 00931, USA*

REVIEW

In this paper we review recent computational insights into the oxidation of graphene, the reduction of graphene oxide, and the molecular models and electronic structures of graphene oxide. First, we will set the stage by giving a brief overview of recent exciting experimental progresses in chemistry of graphite oxide and graphene oxide. Then, we will discuss computational efforts to understand oxidation mechanisms of graphene. Next, we will examine computational efforts to elucidate the molecular and electronic structures of graphene oxide. Further, we will interrogate the reduction mechanisms of graphene oxide. In the end, we provide a perspective how the computational and experimental efforts will converge on the chemistry of graphene oxide.

Keywords: Graphene, Electronic Structure, Molecular Structure.

CONTENTS

---

*Author to whom correspondence should be addressed.

1. INTRODUCTION

When sp^2-carbon atoms are arranged into two-dimensional fused hexagons, they form a single-atom-thick allotrope of carbon: graphene. Graphene has been known as the building block of graphite for more than 60 years,[1] but its experimental isolation was only achieved in 2004.[2] Despite its short history of realization, graphene has attracted much attention because of its extraordinary structural, mechanical, and electronic properties, which make graphene and its derivatives ideal for diverse applications such as energy-storage capacitors, sensors, and transistors.

The large scale production of high-quality graphene is still very challenging. Several laboratory methods have been proposed, each with its own advantages and disadvantages.[2–5] Among them, the chemical reduction of graphene oxide yielding chemically converted graphene

Xingfa Gao received his Ph.D. from Institute of High Energy Physics, Chinese Academy of Sciences in 2006. Then, he did his postdoctoral work in Department of Theoretical and Computational Molecular Science, Institute for Molecular Science, Japan from 2006 to 2010. Currently, he is a postdoctoral research fellow in Department of Physics, Applied Physics, and Astronomy, Rensselaer Polytechnic Institute, USA. Both his Ph.D. and post-doctoral work concerned the theoretical study of carbon conjugated materials, including their structural, electronic and magnetic properties, their reaction mechanisms and design, and the development of corresponding chemical graph models. Besides computations, he is now getting involved in the development and implementation of HF-DFT orbital hybrid methods.

De-en Jiang received his BS and MS degrees in Chemistry from Peking University. He then pursued his Ph.D. study at University of California, Los Angeles under the guidance of Professor Emily A. Carter (now at Princeton University). After visiting Princeton University for one year to finish up his doctoral research with Professor Carter, he received his Ph.D. degree in chemistry from UCLA in 2005. Then he joined Oak Ridge National Laboratory first as a postdoctoral research associate and then became a research staff member in 2006. His research interest lies in applying state-of-the-art computational methods to important chemical systems and problems. His recent studies have dealt with topics such as reactivity and magnetism of nanographenes, porous graphene for gas separations, and geometry and electronic structure of nanoclusters. In 2009, he won ORNL's Early Career Award for scientific achievement.

Dr. Yuliang Zhao is a Professor and Director of Chinese Academy of Sciences Key Lab for Biomedical Effects of Nanomaterials and Nanosafety. His research interests mainly focus on nanotoxicology, cancer nanotechnology and theoretical studies on nanostructures and their interactions with biosystems. He has published about 190 peer reviewed papers (about 140 papers at international journals and 50 papers at Chinese journals). He is serving as Associate Editors for Biomedical Macrodevices (USA), Journal of Nanoscience & Nanotechnology (USA), and Particles & Fiber Toxicology (UK).

Shigeru Nagase, born in 1946 in Osaka, Japan, received his Ph.D. degree from Osaka University in 1975. After working as a postdoctoral fellow (1976–1979) at the University of Rochester and at Ohio State University, he returned to the Institute for Molecular Science in 1979. He became an Associate Professor at Yokohama National University in 1980 and was promoted to Professor in 1991. In 1995, he moved to Tokyo Metropolitan University as Professor. Since 2001, he has been a Professor at the Department of Theoretical and Computational Molecular Science, Institute for Molecular Science. He has great interest in developing efficient theoretical methods to investigate novel molecules and reactions through close interplay between theoretical predictions and experimental tests.

Professor Shengbai Zhang is Professor, Physics, Applied Physics, and Astronomy, Gail & Jeffrey L. Kodosky '70 Senior Constellation Chair in Physics, Information Technology, and Entrepreneurship, Rensselaer Polytechnic Institute. He is a quantum physicist renowned for his computational modeling and study of defects in semiconductors. He received his Ph.D. degree in Physics from the University of California at Berkeley in 1989. He worked as a Postdoctoral Research Fellow at Xerox Palo Alto Research Center for two years and then as a Scientist and Senior Scientist at the US Department of Energy's National Renewable Energy Laboratory for nearly seventeen years, before joining Rensselaer in January 2008. Much of his recent research focuses on providing scientific underpinning to break the technology barriers for alternative energies such as photovoltaics and energy storage. He has also conducted extensive research in nanosciences. Professor Zhang is a Fellow of the American Physical Society.

Dr. Zhongfang Chen is an Associate Professor in the Department of Chemistry, University of Puerto Rico (UPR), Rio Piedras campus. He earned his B.Sc. (organic chemistry, in 1994), M.Sc. and Ph.D. (physical chemistry, in 1997 and 2000, respectively) at Nankai University, Tianjin, P.R. China. In late 1999, he began to work in Germany with Andreas Hirsch (Universität Erlangen-Nürnberg) and Walter Thiel (Max-Planck-Institut für Kohlenforschung in Mülheim/Ruhr) as a postdoc, under the support of Alexander von Humboldt foundation and Max-Planck society. He joined Paul V. R. Schleyer's group in late 2002, but physically remained in Erlangen until his final move to the University of Georgia (UGA) in October of 2003. From 2006 he served as an Associate Research Chemist at UGA, then from 2008 he had a short stay at Rensselaer Polytechnic Institute as a Research Associate Professor before his further move to UPR in the fall. His main research is to apply modern computational tools to design new materials with novel chemical bonding and desired properties, and to investigate rules and trends in chemistry. His research areas are rather broad, including one-dimensional nanomaterials (nanotubes, nanocables, peapods, graphene nanoribbons, etc), novel materials for hydrogen and lithium storage, fullerenes, endohedral metallofullerenes and related endohedral clusters, aromaticity of spherical molecules and clusters, molecules with novel chemical bonding, and novel nanocatalysts, etc. He enjoys his extensive collaborations with peer experimentalists and theoreticians. So far, he has given over 80 lectures around the world, and contributed over 120 papers, which gained him ca. 2500 citations and a H-index of 28.

(CCG) is rather appealing: it is cheap and easily scalable to a high-volume production. Particularly, this solution-based approach is well-suited for chemical modification and subsequent processing. Consequently, the reduction of graphene oxide is widely used for device fabrications, such as the preparation of graphene-based composites, thin films, and paper-like materials.[3] No doubt the chemical processes regarding graphene oxide is one of the most active branches of the rapidly emerging subject—graphene chemistry.

Figure 1 summarizes the chemical procedures for synthesizing chemically converted graphene from graphite. Three steps are mainly involved. The first is the oxidation of graphite. In this process, oxygen-containing groups are introduced on graphite surfaces and in between graphite carbon layers, which converts hydrophobic graphite to hydrophilic graphite oxide. The latter oxygen-containing groups severely reduce the inter-layer stacking forces, which makes carbon layers of graphite oxides loosely packed and susceptible to exfoliation. The second step is the exfoliation of graphite oxide, which gives single-layered graphene oxide. The exfoliation is usually carried out in aqueous solutions with the aid of sonication in an ultrasonic bath. The last step is the chemical reduction of graphene oxide, which yields chemically converted graphene. All chemically converted graphenes have residual oxygen-containing groups, so are not pure.

Recently, several reviews have been dedicated to the progresses on the experiments of graphene, graphene oxides and their applications and chemical conversions.[3–11] Similar to other research fields, molecular modeling and computation serve as an indispensable approach besides experiments for graphene research. Here, we will review theoretical studies on graphene chemistry. In particular, we will focus on theoretical insights into the structures of

graphene oxides and the mechanisms of conversions illustrated in Figure 1.

2. EXPERIMENTAL PROGRESSES

2.1. Preparation of Graphite Oxide

Due to the high chemical stability of graphite, highly oxidized graphite can only be realized in harsh reaction conditions, which is usually accomplished in experiments by using strong oxidizing mixtures consisting of one or more concentrated acids and oxidizing materials. The first synthesis of graphite oxide was by Brodie[12] in 1859, who treated graphite repeatedly with the mixture of potassium chlorate ($KClO_3$) and nitric acid (HNO_3). Other two most commonly used approaches were described by Staudenmaier in 1898[13] and Hummers-Offeman in 1958.[14] The Staudenmaier method treats graphite with concentrated sulfuric (H_2SO_4) and nitric acids with potassium chlorate ($KClO_3$), while the Hummers-Offeman method treats graphite with concentrated sulfuric acid, sodium nitrate ($NaNO_3$) and potassium permanganate ($KMnO_4$). Among them, the Hummers-Offeman method,[14] as well as its variants,[15, 16] has been widely used to prepare graphite oxides as the precursors for the further syntheses of graphene oxide and graphene because of its high oxidizing efficiency. Through analyzing the step by step preparation of graphite oxide in nitric acid media, Mermoux and Chabre[17] proposed that the graphite oxide is formed via the hydrolysis of an intermediary compound resulted from the overoxidation of nitric-acid-intercalated graphite.

2.2. Properties of Graphite Oxide

Graphite oxide appears yellowish-brown in solid and is strongly hydrophilic and hygroscopic; when dispersed in
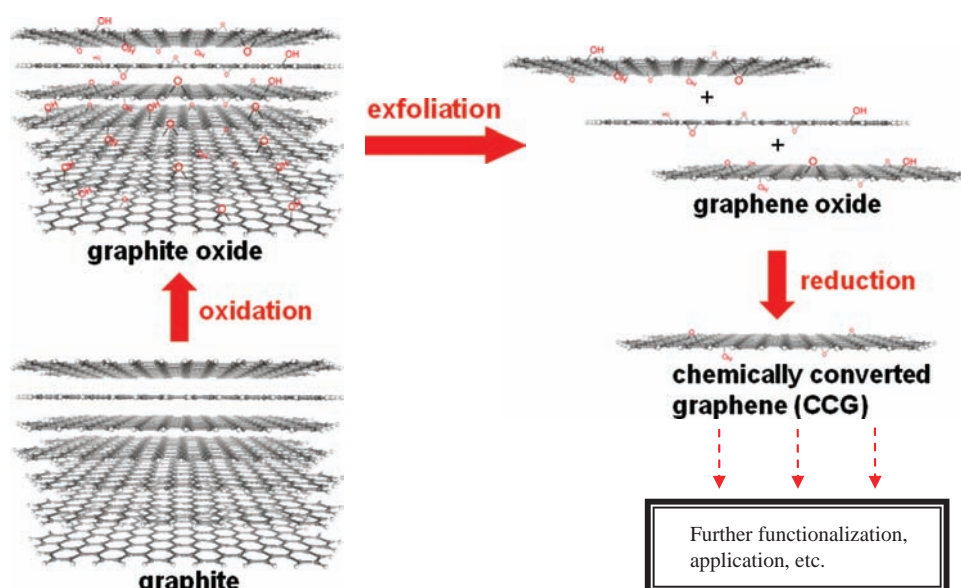
Fig. 1. Schematic illustration for the chemical processes from graphite to chemically converted graphene.

water, the resulting stable colloid has a dark brown color.[14] Graphite oxide is nearly amorphous without a constant C/O composition in nature; its stoichiometry varies with the method of preparation, the pristine graphite, and the particle size.[18, 19] Graphite oxide still possesses a two-dimensional layered structure; however, unlike the pristine graphite which is atomically ordered with an interlayer distance of ∼0.34 nm, the interlayer distance for graphite oxide is much "thicker" due to the presence of oxygen-containing groups: X-ray diffraction (XRD) experiments have suggested that the distance varies with the amount of absorbed water, with value ∼0.62 nm for "dry" samples and 1.2 nm for hydrated samples.[20] Due to the strong hydrophilicity and weak interlayer interaction, graphite oxide can be facilely exfoliated to single-layered graphite oxide, i.e., graphene oxide, via sonication.

Graphite oxide is thermally unstable. It starts to lose mass upon heating to above 60–80 °C, presumably due to leaving of absorbed water; the major mass loss occurs at ∼200 °C, presumably due to decompositions of labile oxygen-containing functionalities that yield carbon monoxide, carbon dioxide and water steam.[20] Graphite oxide has a weak oxidbillity and acidity. Using $NaBH_4$ and hydroquinone as reducing agents, respectively, Bourlinos et al.[21] reduced graphite oxide back to graphite; these authors also successfully modified the graphite oxide surfaces with series of primary aliphatic amines and amino acid.

Due to the highly hydrophilic nature and weak interlayer interactions, graphite oxide readily forms stable colloidal suspensions of nanoplatelets with nanometer scale thickness in water.[22] Ruoff et al.[23] found that under a mild ultrasonic treatment, the suspended graphite-oxide sheets can completely exfoliate to form dispersion of single-layered graphite oxide, namely graphene oxide, which can remain stable for ∼ a month at the concentration of 1 mg/mL; atomic force microscopy (AFM) showed that the exfoliated graphite oxides have a uniform thickness of ∼1 nm and a mean lateral dimension of 1 μm. However, the strong hydrophilicity prohibits the dispersion of graphite oxide in non-aqueous solvents. To exfoliate graphite oxide in organic solvents, Ruoff et al.[24] treated graphite oxide with organic isocyanates, and successfully exfoliated the isocyanate-treated graphite oxide into functionalized graphene oxide nanoplatelets which can stably dispersed in polar aprotic solvents. Cai and Song[25] found that under strong ultrasonic treatment, oxide of expanded graphite can exfoliate in polar organic solvent N,N-dimethylformamide (DMF) and form a stable non-aqueous dispersion.

The colloidal dispersion of as-made individual graphene oxide has been made into well-ordered macroscopic structures such as graphene oxide paper. Ruoff et al.[26] demonstrated that under a directional flow induced by vacuum filtration, the colloidal graphene oxide can interlock in a near-parallel manner, generating a paper-like material that is remarkably stiff and much stronger than its nanotube counterpart (Fig. 2).

The extensive presence of oxygen-containing groups on the lateral sides of graphene oxide greatly enhances it band gap; as a result, graphene oxide is electrically insulating and can not be directly used as a conductive material. The existence of these groups also makes graphene oxide thermally unstable, which undergoes pyrolysis at elevated temperatures.[20]
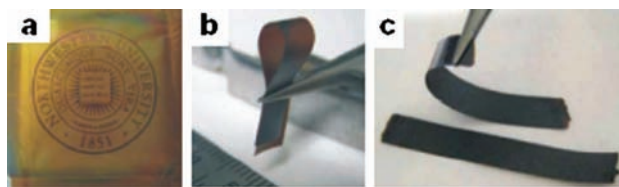
4

J. Comput. Theor. Nanosci. 8, 1–17, 2011

Fig. 2. Digital camera images of graphene oxide paper. (a) ∼1 mm-thick (the Northwestern University logo is beneath the paper); (b) folded ∼5 mm-thick semitransparent film; (c) folded ∼25 mm-thick strip. Reprinted with permission from [26], D. A. Dikin et al., *Nature* 448, 457 (**2007**). © (2007), Nature Publishing Group.

2.3. Methods to Chemically Convert Graphene Oxide to Graphene

Various methods have been used to convert graphene (graphite) oxide to graphene (graphite) by removing the oxygen-containing groups and restoring the carbon skeleton.[20, 21, 27] In a graphene oxide dispersion (100 mg graphene oxide + 100 mL water), Ruoff et al., added hydrazine hydrate (1.00 mL, 32.1 mmol) and heated the mixture in an oil bath at 100 °C under a water-cool condenser for 24 h and found that the brown-colored dispersion turns black and the reduced products irreversibly aggregate and eventually precipitate.[20] They carefully compared the solid-state magic angle spinning (MAS) NMR spectra of the pristine graphene oxide and the hydrazine-treated sample, and found that the peaks at 57, 68 and 188 ppm in graphene oxide ^{13}C NMR spectrum, which represent the ^{13}C nuclei in the epoxide, hydroxyl and carbonyl groups, respectively, are greatly reduced in the spectrum of hydrazine-treated sample; moreover, the peak at 130 ppm in graphene oxide spectrum, which represents un-oxidized carbons, remains in the spectrum of hydrazine-treated sample but with a broadening and chemical shifting due to the variation of chemical environment. The elemental analyses showed that the C/O ratio (2.7) in the pristine graphene oxide is dramatically increased (to 10.3) in the hydrazine treated sample. All these measurements revealed that hydrazine partially removed the oxygen-containing groups from graphene oxide. The electrical conductivity measurements (for the compressed-powers) showed that the conductivity of the reduced graphene is about five orders of magnitude better than that of pristine graphene oxide. However, the lattice defects introduced in the graphene oxide can not be repaired in this chemical reduction process.

Besides hydrazine,[9, 16–18] other reducing agents such as hydroquinone,[21] $NaBH_4$,[21] and hydrogen[28, 29] have also been used to partially remove oxygen-containing groups and increase the electric conductivity. Recently, Fan et al.[30] demonstrated a green method for graphene preparation without using the hazardous hydrazine: the reduction of graphene oxide and the dispersion of the reduced graphene can be realized in a strong alkaline condition.

In addition to chemical reduction, electrochemical reduction[28, 31] and thermal treatment[32, 33] have also proven to be efficient for deoxygenation. Becerril et al.[34] compared the electric conductivities of the graphene oxide treated with thermally annealing (1100 °C) or hydrazine, and found that thermally annealing gives rise to more efficient deoxygenation. Recently, Yang et al.[35] also compared the graphene oxide films after hydrazine or heat treatment and reached the similar conclusion that the heat treatment (900 °C) in an ultra-high vacuum condition yields product with larger C/O ratio (∼1.41 vs. ∼8.8).

3. OXIDATION MECHANISMS OF GRAPHENE

3.1. Reaction of O_2 with the Armchair Edge of Graphene

Using **1** as the model (Fig. 3(a)), Sendt and Haynes[36] thoroughly studied the chemical reactions of O_2 on the dehydrogenated armchair-edge of graphene by means of density functional theory (DFT) computations. Calculations at the B3LYP/6-31G(d) level of theory showed that the C2–C3 (**1**) bong length (1.24 Å) is equal to that of the triple bond in benzyne. Therefore, the dehydrogenation converts the edge to triple bonds (Fig. 3(a)), satisfying the octet rule. The reaction energy profile for O_2 chemisorption on the C2–C3 (Fig. 3(b)) suggests that the formation of quinone structure IV is thermodynamically favorable, with a small energy barrier (18 kJ/mol) and a large exothermicity (−578 kJ/mol). Structures II and III exist on the transformation path, but both intermediates are unlikely to have a significant lifetime because of the small reaction energy barriers of TS2 and TS3 (Fig. 3(b)). The reaction occurs mainly at triplet state from I to II, whereas at singlet from III to IV. The surface crossing from triplet to singlet occurs near the geometry of TS2, which the triplet and singlet species have the same energy. Quinone structure IV is possible to undergo two successive CO desorptions to give graphene diradical VI. As shown in Figure 3(c), the formation of the five-membered ring ketone (V) from IV (i.e., the first CO desorption) is 85 kJ/mol endothermic with an energy barrier of 296 kJ/mol. However, the second CO desorption is approximately 435 kJ/mol endothermic with a significant high barrier and a negligible reverse barrier. Therefore, the second CO desorption occurs only at high temperatures. The ketone structure (V) can also be formed via a stepwise CO desorption as shown in Figure 3(d).

For model **2** that has neighboring triple bonds (Fig. 3(a)),[36] the five-membered ring lactone (XI) formed through oxygen migration of quinone (VIII) was found to be the most stable structure identified on the potential energy surface (Fig. 3(e)). All gasification channels from VIII are endothermic with high reaction energy barriers.
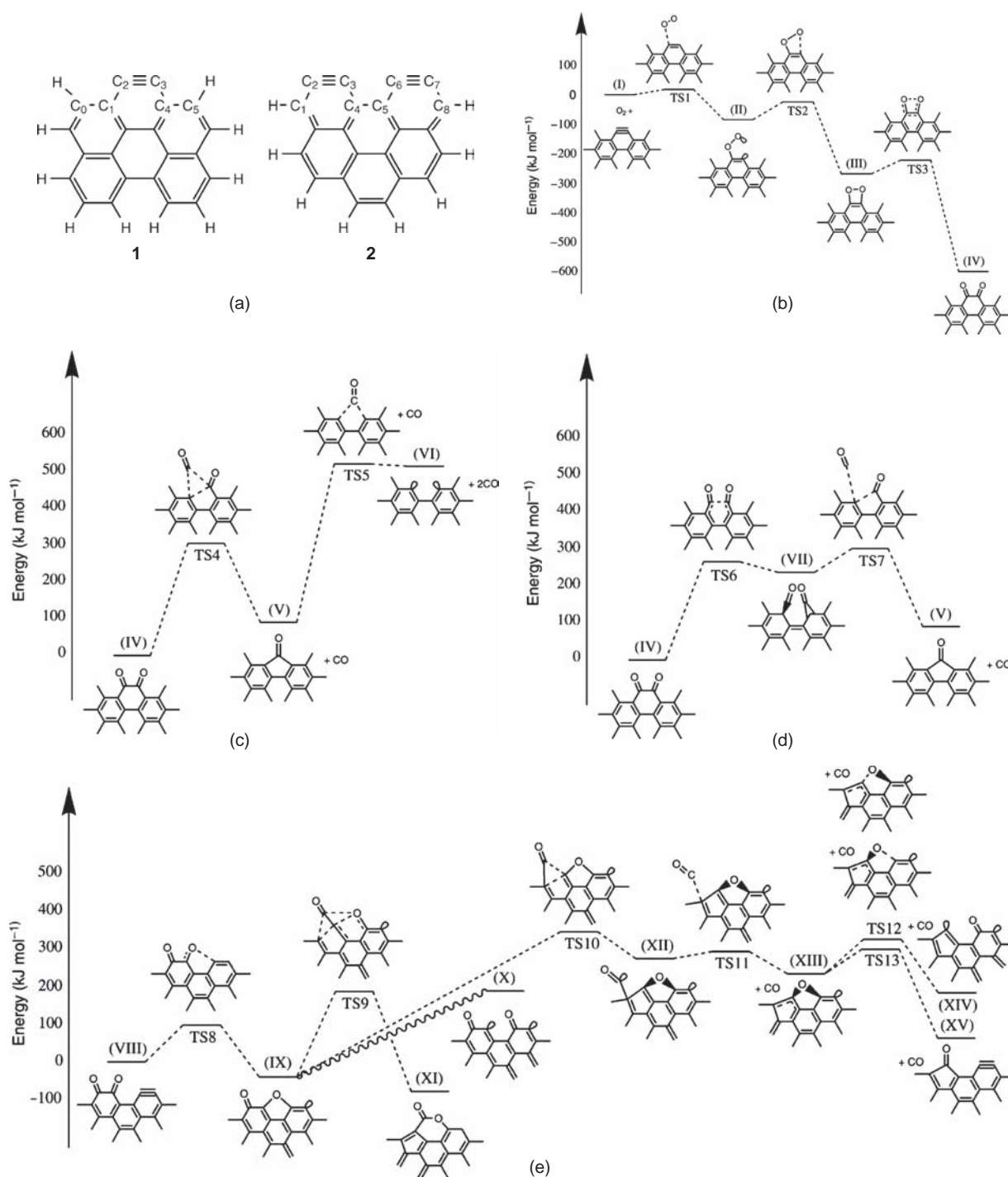
Fig. 3. Potential energy surface for O_2 chemisorption on **1**, calculated at the level of B3LYP/6-31G(d). Reprinted with permission from [36], K. Sendt and B. S. Haynes, *Proc. Combust. Inst.* 30, 2141 (**2004**). © (2004), Elsevier (including Academic Press).

The authors also studied the chemisorption of O_2 across two neighboring triple bonds, i.e., C3 and C6 of **2** (Fig. 3(a)).[37] Diketene structures in addition to lactone were found as the stable chemisorption species. However, further gasifications from these stable species are kinetically unfavorable, similar to the case of O_2 chemisorption on the same triple bond of **1** or **2** (Fig. 3(a)).

3.2. Unified O_2 Gasification Model of Graphene Flakes

Zhu et al.[38] proposed oxidation-gasification model for nanographene with bare zigzag edges (Fig. 4). Owning to the large exothermicity for O_2 chemisorption on the bare edges (Fig. 4(a)), nearly all the edge sites can chemisorb
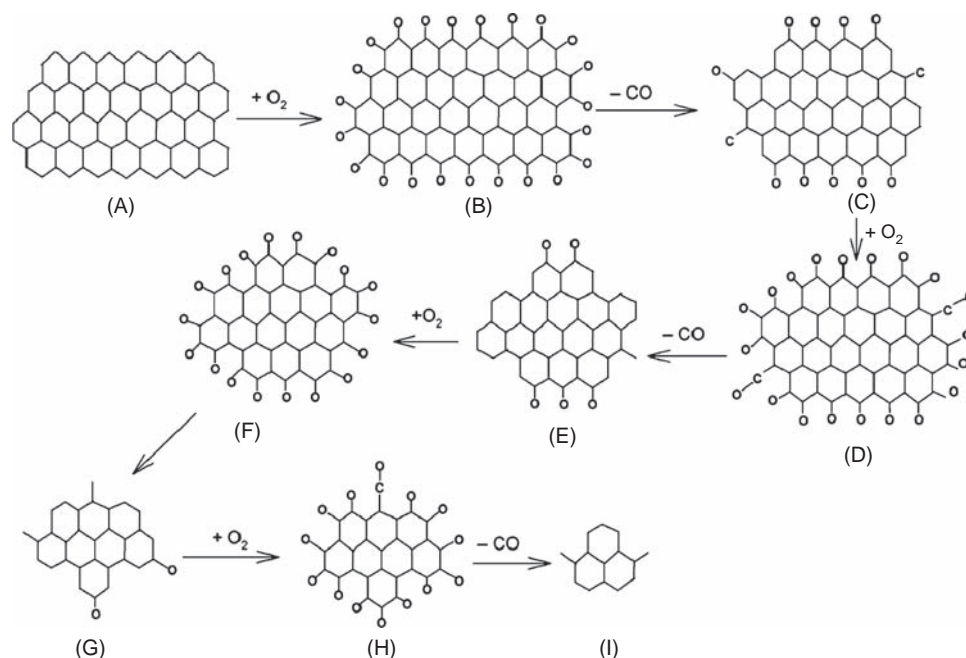
6

J. Comput. Theor. Nanosci. 8, 1–17, **2011**

Fig. 4. Models for the reaction of O_2 with zigzag-edged graphene. Reprinted with permission from [36, 38], Z. H. Zhu et al., *Energy Fuels* 16, 1359 (**2002**). K. Sendt and B. S. Haynes, *Proc. Combust. Inst.* 30, 2141 (**2004**). © (2004), American Chemical Society.

O atoms (B). The *o*-quinone C−C bonds of B are cal-culated to have lower bond strengths, and thus provide rational starting points for gasification. The CO desorption occurring on B reduces the carbon surface and results in new active sites on C. Therefore, more O atoms will be captured to form new *o*-quinone units in D. As the reaction proceeds from D to E to F to G to H to I, the graphene flake shrinks until it is completely consumed.

The above *o*-quinone-oriented O_2-gasification model for graphene flakes is applicable in conditions where the O_2 partial pressures (P_{O2}) are medium. Figure 5 shows the unified model for graphene flakes at different P_{O2}.
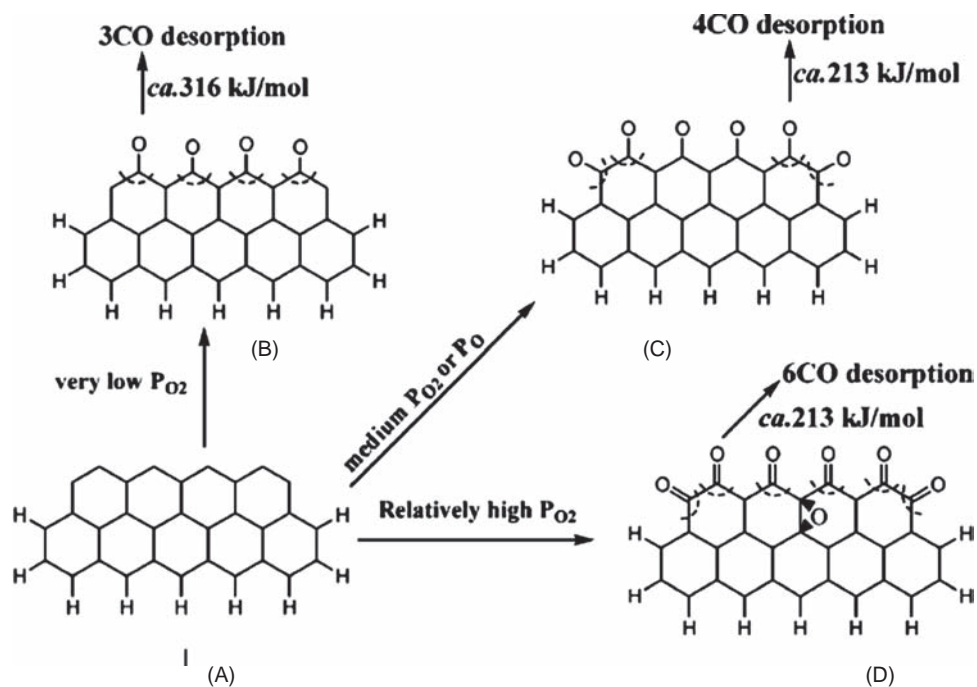

Fig. 5. The unified O_2 gasification mechanism proposed by Zhu et al. Reprinted with permission from [36, 38], Z. H. Zhu et al., *Energy Fuels* 16, 1359 (**2002**). K. Sendt and B. S. Haynes, *Proc. Combust. Inst.* 30, 2141 (**2004**). © (2004), American Chemical Society.

At a low P_{O_2}, *o*-quinone units, which are more subject to CO desorption, will not form. Instead, O_2 dissociatively chemisorbs on A, giving B with semiquinone units (Fig. 5). The release of CO from these semiquinone structures requires more energy than that from *o*-quinone due to the larger bond energy of semiquinone (316 kJ/mol). At medium P_{O_2}, the reaction proceeds via the mechanism of Figure 4, forming *o*-quinone units as gasification centers. If the P_{O_2} is further increased, the formation of epoxy groups on the basal plane of graphene flake will occur, which add more active sites and accelerate the gasification process.

3.3. Reaction of O_2 with Vacancy Defect of Graphene Flakes

CO is the main products in the above gasification models concerning the reactions of O_2 with graphene edges. However, it is CO_2 rather than CO that was experimentally observed for complete combustion under atmospheric oxygen pressure. To explain this, Carlsson et al.[39] proposed a two-step oxidation mechanism, which starts from the vacancy defects in graphene basal plane (Fig. 6). As reported by others,[40, 41] the dissociative adsorption of O_2 on the basal plane of defect-free graphene results in epoxy groups. This process is highly endothermic and thermodynamically disfavored (see route G of Fig. 6(a)), in agreement with the experimentally observed inertness of graphene basal plane towards O_2 at low temperatures.[42] However, if vacancies exist on graphene, these defect sites provide very reactive sites for oxidation. Route I of Figure 6(a) illustrates the reaction energy profile for O_2 with a four-atom carbon vacancy (V4) of graphene. To minimize the dangling bonds, V4 rearranges to form three pentagons as the metastable structure.[43] This structure strongly reacts with molecular O_2 to form ether (C−O−C) or carbonyl groups, releasing a large amount of heats. The addition of oxygen can proceed until complete saturation.

The first step of the Carlsson mechanism[39] is the reaction of O_2 with the bare vacancies of graphene, the oxygen-saturated sites are less reactive than bare vacancies but still more reactive than defect-free graphene. The second step of this mechanism (Fig. 6(b)) is that additional oxygens attach these oxygen-saturated structures above the critical temperature. These reactions are also exothermic and form oxygen-rich structures like lactone (C−O−C=O) and the anhydride (O=C−O−C=O). The lactone either releases CO_2 or forms anhydride by a further O_2 adsorption, whereas anhydride rapidly decomposes to CO_2. The CO_2 desorption creates new sites for O_2 dissociative addition, driving the etching reaction further.

3.4. The Cooperative Oxidation Mechanism of Graphene

Figure 7 shows the optical microscope image of partially oxidized highly oriented pyrolytic graphite (HOPG). The most oxidized region, represented by bright area, suggests the formation of line defects during the oxidation process. The crack down of graphene, directly related to the oxidation, was also observed. To rationalize the observed fault lines and cracks of graphene oxide, Li et al. proposed the cooperative oxidation mechanism,[44] which was illustrated on a finite graphene model—coronene molecule (Fig. 8). The addition of a single O atom to coronene forms an epoxy group (Fig. 8(a)) with an exothermicity of ∼2.4 eV;
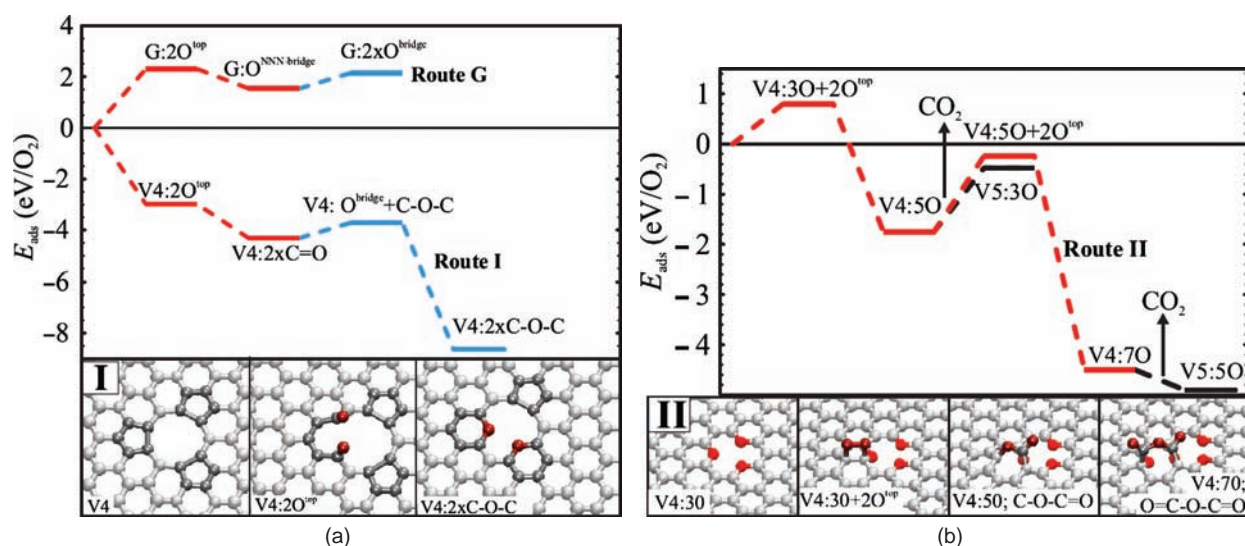

Fig. 6. Calculated reaction energy profiles for O_2 and graphene. (a) The adsorption energy for dissociative O_2 adsorption on the defect-free graphene (route G) and at a bare four-atom (V4) vacancy (Route I). (b) The adsorption energy for dissociative O_2 adsorption at an oxygen-saturated V4:3O vacancy (Route II). Reprinted with permission from [39], J. M. Carlsson et al., *Phys. Rev. Lett.* 102, 166104 **(2009)**. © (2009), American Physical Society.
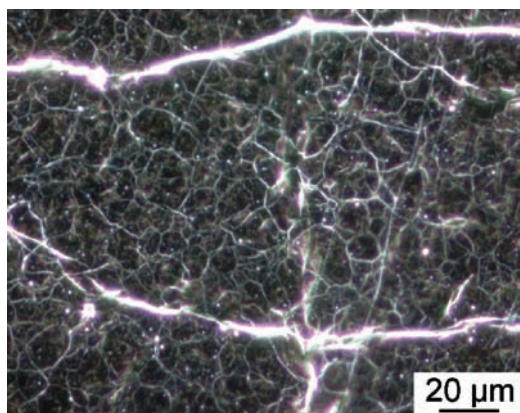
Fig. 7. An optical microscope image of partially oxidized highly oriented pyrolytic graphite. Reprinted with permission from [44], J.-L. Li et al., *Phys. Rev. Lett.* 96, 176101 (**2006**). © (2006), American Physical Society.

simultaneously, the epoxy C−C bond is stretched from 1.42 Å (the pristine carbon lattice) to 1.58 Å. The addition of the second O atom takes place more preferably at the opposite site of the epoxy group (Fig. 8(b)). Importantly, such a cooperative unzipping pattern increases the formation energy of the second epoxy ground addition due to the confirmation changes, and the C−C bonds of both epoxy units become open. The authors found that this unzipping configuration (Fig. 8(b)) is thermodynamically more favorable than any other configurations by ∼1.2 eV. Similar preference of this unzipping configuration was also found for the reaction of O with larger model of graphene flake and the sidewall of single-walled carbon nanotubes. The unzipping process can proceed continuously by further cooperative formation of open epoxy groups (Figs. 8(c and d)). Given that open epoxy structure is significantly weaker than
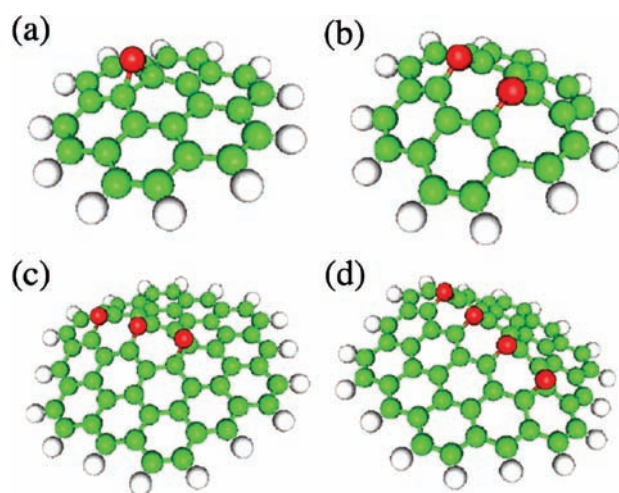
closed-ring structures, the cooperative oxidation mechanism not only explains the observed of line faults and cracks of graphene oxide but also gives insight into chemical cutting of carbon nanotubes via oxidation reactions.

3.5. Oxidative Cutting of Graphene

It was found that the mechanical strength of graphene is not critically affected by introducing epoxy frauds (thus forming linear frauds of ethers) during oxidation, but only weakened by ∼16%.[45] The probable reason is that the graphene sheets still remain linked by the oxygen atoms after the rupture of the C−C bonds. Thus the cooperative mechanism for the formation of linear frauds can not eventually account for the break up of graphene oxides. To better rationalize how graphene is cut during oxidation, Li et al. theoretically examined the subsequent oxidation process of graphene oxide after the formation of linear ethers (Fig. 9(a)), and also proposed a new "tear-from-the-edge" mechanism.[46]

Through DFT computations, Li et al. found that the formation of epoxy-pair structure on graphene basal plane can further activate the carbons where the ethers are attached. For example, the epoxy-pair structure of Figure 9(b) was calculated to be 2.71 eV lower in energy than the structure with the second epoxy group added far from the epoxy chain. Moreover, the formation of an epoxy pair neighboring an already existing epoxy pair was calculated to be 0.78 eV more favorable than that forming an isolated epoxy group, which suggests that creating new epoxy pair is still energetically favored even with the existing epoxy pairs. For a short epoxy chain, the formation of an epoxy pair by adding a new O to an existing epoxy was comparable in energy (within 0.1 eV) to the extension of the ether chain by adding a new O on fresh carbon–carbon bond neighboring existing ether. Further computations revealed that a carbonyl pair has an even lower energy than an epoxy pair by 0.48 eV and that an epoxy pair can transform to a carbonyl pair with an activation energy of 0.76 eV. A neighboring epoxy pair can further
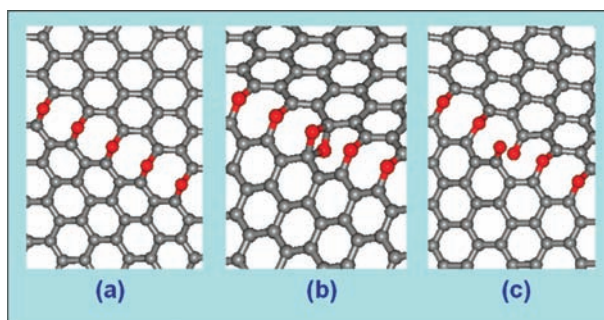
Fig. 8. Coronene molecules attached with (a) one, (b) two, (c) three and (d) four epoxy groups, respectively. Reprinted with permission from [44], J.-L. Li et al., *Phys. Rev. Lett.* 96, 176101 (**2006**). © (2006), American Physical Society.

Fig. 9. Oxygen chains on graphene. (a) A graphene sheet with an epoxy chain. (b) An epoxy pair or (c) a carbonyl pair is formed in the epoxy chain. Reprinted with permission from [46], Z. Li et al., *J. Am. Chem. Soc.* 131, 6320 (**2009**). © (2009), American Chemical Society.
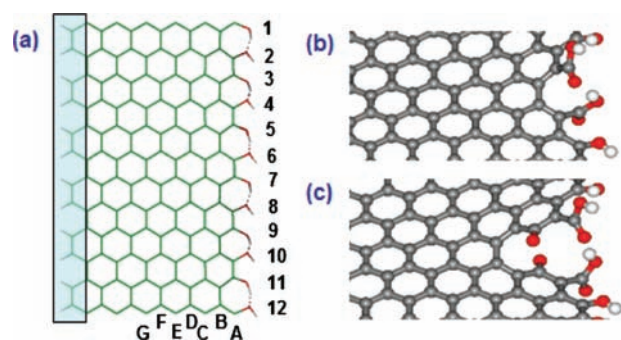
Fig. 10. Tearing graphene from the edge. (a) Geometric model to describe a graphene edge. Atoms in the square area were frozen during geometry relaxation. (b) A carbonyl pair at the edge. (c) Another carbonyl pair formed one step inward. Reprinted with permission from [46], Z. Li et al., *J. Am. Chem. Soc.* 131, 6320 (**2009**). © (2009), American Chemical Society.

lower this activation energy to 0.45 eV, which reflects a substantial reaction rate for the transition from epoxy pair to carbonyl pair. The simultaneous transformation from two neighboring epoxy pairs to carbonyl pairs has a relatively high activation barrier (1.07 eV). However, after completing the first transition, the conversion of the second epoxy to carbonyl encounters only a small barrier of 0.26 eV. Therefore, combining the cooperative formation of linear ethers by Li et al.[44] and the subsequent formation of epoxy pairs and carbonyl pairs by Li et al.,[46] we have a more thorough, atomistic-scaled insight into the fracture of graphene caused by oxidation.

The possibility of directly forming carbonyl pairs by breaking the C−C bonds at graphene edges inspired Li et al. to examine the feasibility of a new oxidation-cutting progress, namely "tear-from-the-edge" progress,[46] by DFT computations. In the slab model of Figure 10(a), the leftmost carbons were saturated by hydrogens and were frozen during the calculations, whereas the remaining carbons were allowed to be relaxed. The rightmost carbons were saturated by hydroxyl groups. It was found that the formation of carbonyl pair at positions A6 and A7 (Fig. 10(b)) is more favorable in energy (1.08) than that at positions B7 and B8. However, the formation of another carbonyl pair one step inward (Fig. 10(c)) is energetically less favorable than carbonyl pairs formed at new edge carbons. Therefore, the "tear-from-the-edge" progress was unlikely to proceed and fully cut the graphene sheet. The failure of the "tear-from-the-edge" mechanism in turn indicates epoxy pairs to be the critical intermediate species responsible for the experimentally observed oxidation-cutting phenomena.

4. EFFORTS IN ELUCIDATING THE STRUCTURES OF GRAPHENE OXIDE

4.1. Structural Models for Graphene Oxide

Extensive attempts have been made to determine the structure of graphite oxide. However, due to its
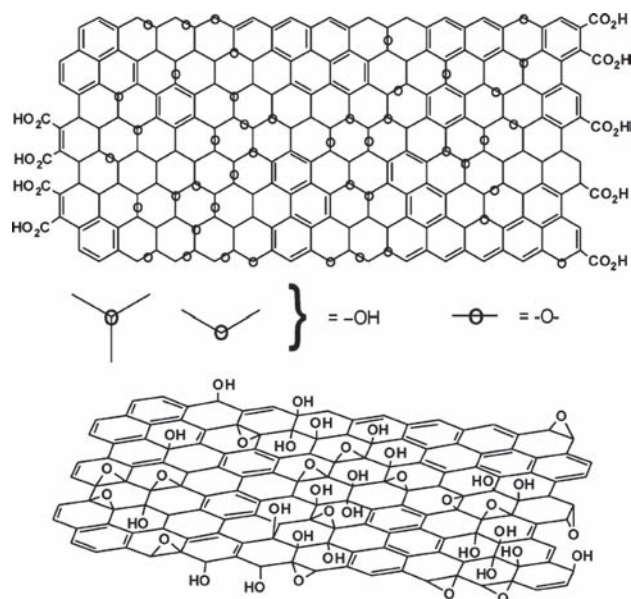

Fig. 11. Graphene oxide model proposed by Lerf, et al. Reprinted with permission from [6], D. R. Dreyer et al., *Chem. Soc. Rev.* 39, 228 (**2010**). © (2010), Royal Society of Chemistry.

non-stoichiometric and nearly amorphous nature, the precise structure of graphite oxide is still ambiguous. So far, it is generally accepted that four oxygen-containing groups are present in graphite oxide, and connected by sp^2-carbon atoms: epoxy and hydroxyl groups on the basal planes, as well as carbonyl and carboxyl groups on the peripheries. This picture was supported by the very important experiment recently made by Cai et al.[47] Using ^{13}C-enriched graphite oxide prepared by the Hummers-Offeman method,[14] the authors confirmed the presence of the four oxygen-containing groups and for the first time proved their connectivity in graphite oxide, by measuring the high-resolution solid-state ^{13}CNMR spectra with magic angle spinning.

Before Cai et al.'s experiment, six structural models for graphite oxide had been proposed by Hoffmann,[48] Ruess,[49] Scholz et al.,[50] Nakajima et al.,[51,52] Lerf et al.[42–45] and Szabó et al.[18] Among them, only the Lerf's (Fig. 11) and Szabó's models (Fig. 12) meet the requirement of above mentioned experimental results. Recently, Casabianca et al.[53] computationally studied the ^{13}C solid-state NMR for diverse graphene-oxide model clusters and found that only the model by Lerf et al. can best reproduce the experimentally measured NMR.

4.2. The Stability of Graphene Oxide with Respect to Oxygen Coverage

Boukhvalov and Katsnelson[54] theoretically investigated the structures of graphene oxide with various coverages by epoxy and hydroxyl groups, as well as their ratio with respect to thermodynamic stability. The chemisorption of
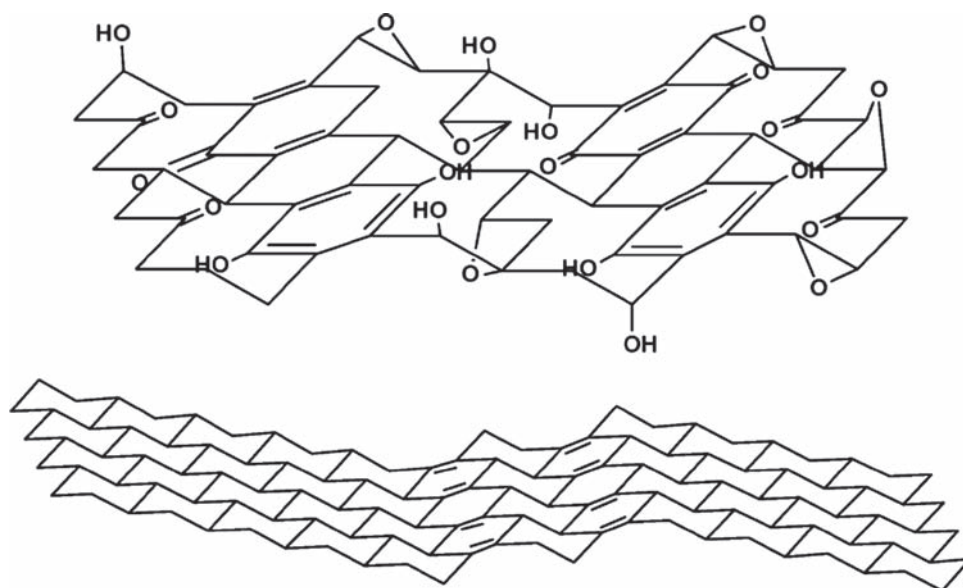
REVIEW

10

Fig. 12. Graphene oxide model proposed by Szabó, et al. Reprinted with permission from [6], D. R. Dreyer et al., *Chem. Soc. Rev.* 39, 228 (**2010**). © (2010), Royal Society of Chemistry.

two oxygen atoms or two hydroxyl groups on the eight-carbon-atom supercell corresponds to oxygen coverage of 25%.

The addition of oxygen atom and the formation of epoxy group lead to the distortion of graphene skeleton, so the subsequent epoxidation occurs more preferably at the opposite side of the graphene sheet. This can be clearly seen from the thermodynamically most favorable configuration of the supercell covered by four epoxy groups (Fig. 13(a)). The chemisorption energy keeps going more negative with increasing the epoxy coverage, suggesting that all graphene carbon–carbon bonds are subject to epoxidation thermodynamically.

The addition of hydroxyl groups to the supercell results in an even stronger distortion, partially because of the interaction between the hydroxyl groups. In contrast to the case of epoxidation, the hydroxylation energy reaches its minimum when the hydroxyl coverage is 75% (six among the eight carbons are attached with hydroxyls). Figure 13(b) shows the most stable configuration for supercell of graphene with six hydroxyl groups.

Generally both epoxy and hydroxyl groups exist in graphene oxide. Figure 14 shows the typical combination of both groups in the C_8 supercell of graphene. For all these combinations, the calculations suggested that the chemisorption energy per hydroxyl was 60 meV more favorable than that of the pure hydroxyl product with the same coverage, and that the chemisorption energy per epoxy was 30 meV more favorable than that of pure epoxy product with the same coverage. This indicates the thermal preference of the coexistence of both oxygen-containing groups in graphene oxides at coverages between 25% and 75%. However, the chemisorption energy of hydroxyl turns out to be more favorable than that of epoxy when

the coverage is less than 25%. Therefore, it was predicted that graphene oxide with 25% oxygen coverage contains mostly hydroxyl groups, whereas epoxy exists only at the edges. Figures 14(a, e, c and h) show the optimal configurations for graphene oxides with total oxygen (epoxy + hydroxyl) coverages of 25%, 50% and 100%, respectively.
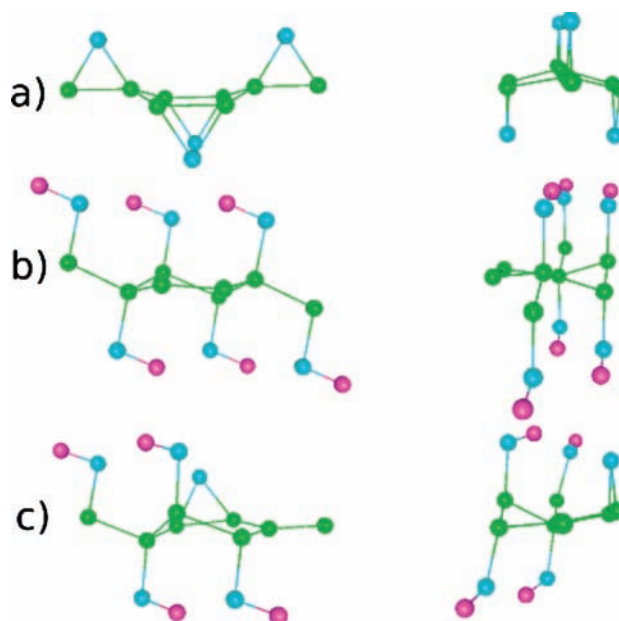

Fig. 13. The most stable configurations of graphene oxides. (a) C_8 unit with only epoxy groups. (b) C_8 unit with only hydroxyl groups. (c) C_8 unit with both epoxy and hydroxyl groups. Reprinted with permission from [54], D. W. Boukhvalov and M. I. Katsnelson, *J. Am. Chem. Soc.* 130, 10697 (**2008**). © (2008), American Chemical Society.

Fig. 14. Graphene oxides. (a-j) C_8 unit attached with both epoxy and hydroxyl groups. Reprinted with permission from [54], D. W. Boukhvalov and M. I. Katsnelson, *J. Am. Chem. Soc.* 130, 10697 (**2008**). © (2008), American Chemical Society.
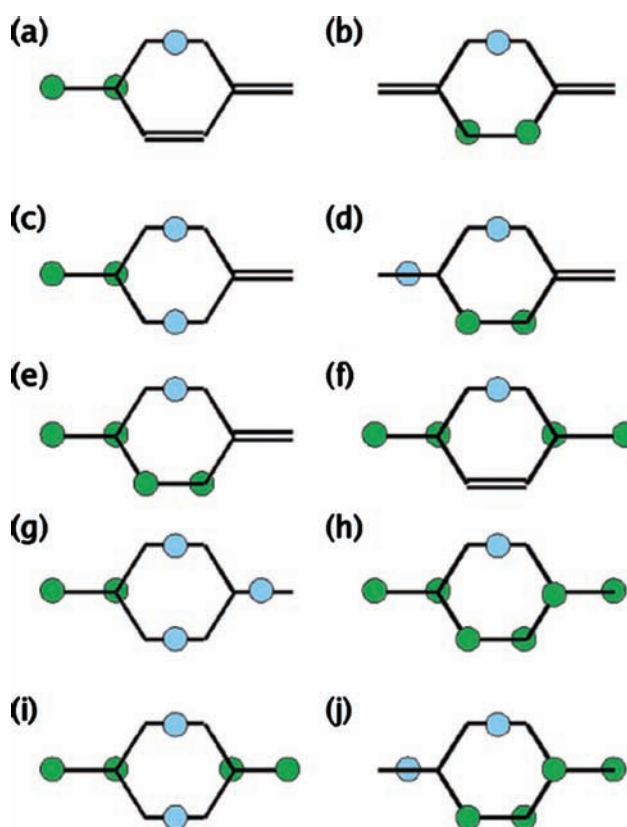
4.3. Stable Periodic Configuration of Graphene Oxide

Yan et al.[55] searched the stable configuration of graphene oxide using periodic boundary conditions with larger super-cells: 5×5 unit cell consisting of 50 carbon atoms. It was found that the energies are lowered considerably when epoxy and hydroxyl groups are grouped together, which is consistent with the results of Boukhvalov et al.[54] Significant energy gains were also found for hydroxyls when they form 1,2-hydroxyl pairs on the opposite site of graphene sheet or form hydrogen bonds with neighboring oxygen atoms.

The stable compositions for fully oxidized graphene oxides, in which all carbon atoms are bonded to epoxy or hydroxyl, have the formulas of $C_6O_2(OH)_2$, $C_4O(OH)_2$ and $C_6O(OH)_4$, with an epoxy to hydroxyl ratio of 1:1, 1:2 and 1:4, respectively. The representative $C_6O_2(OH)_2$ structure (Fig. 15(a)) illustrates the following key features: the 1,2-hydroxyl pairs form chain-like structures to maximize the formation of hydrogen bonds; epoxy oxygens are distributed on the proximate carbons in the same hexagonal rings of the hydroxyl pairs. The fully-oxidized epoxy-only configuration of graphene oxide has epoxy rows on both sides of the basal plane (Fig. 15(b)). After exploring various atomic configurations, Yan et al. concluded that
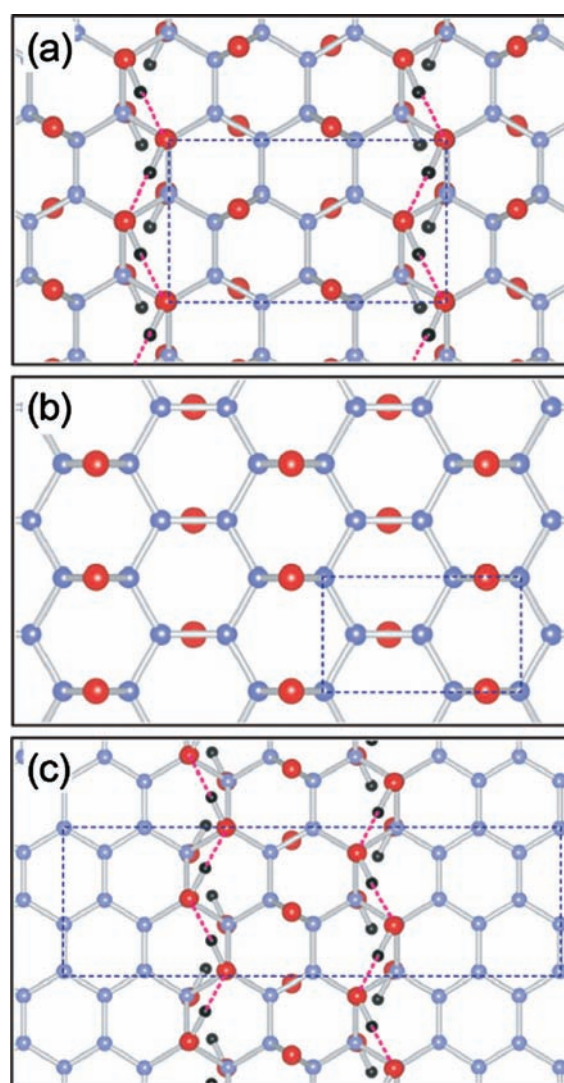

Fig. 15. Structures for graphene oxides. (a) Fully-oxidized phase of $C_6O_2(OH)_2$. (b) Fully-oxidized epoxy-only phase C_2O with epoxy rows on both sides of the basal plane. (c) $C_{24}O_2(OH)_8$ structure with hydroxyl-epoxy strips separated by sp^2 carbons. The dashed rectangles indicate the respective unit cells. The dashed lines indicate the hydrogen bonds in the hydroxyl chains above the basal plane. Reprinted with permission from [55], J.-A. Yan et al., *Phys. Rev. Lett.* 103, 086802 (**2009**). © (2009), American Physical Society.

the most stable periodic structure for partially oxidized graphene as the strips of epoxy-hydroxyl combinations with unoxidized graphene ribbons in between, as exemplified by the structure of $C_{24}O_2(OH)_8$ in Figure 15(c).

5. ELECTRONIC STRUCTURE OF GRAPHENE OXIDE

5.1. Oxidation Induced Band-Gap Opening of Graphene

Boukhvalov et al.[54] and Yan et al.[55] independently studied the variation of energy gaps of graphene oxides with C:O

12

ratios. According to Boukhvalov et al.'s results based on a C_8 unit cell (Fig. 16), the energy gap reduces when the oxidation coverage decreases from "4(OH)+O" to "2(OH)+ O;" when the coverage is further reduced to "2(OH)," the graphene oxide becomes conducting. While Yan et al. suggested that the band gap of graphene oxide depends not only on oxygen coverage but also the arranging pattern of oxygen groups (Fig. 17).[55]

5.2. Consequence of Spin Upon Linear Oxidation of Nanographene

Using molecules **3**, **4** and **5** as models, Gao et al.[56] theoretically studied the structures and spins of nanographenes unzipped by linear formation of epoxy groups. These molecules are known as "all-benzenoid" and are highly stable because all their carbons can be put in isolated sextets (i.e., circle as shown in Fig. 18), according to Clar's sextet rule.

The linear oxidation of **3** along the dash line leads to five products (i.e., **3a**–**e**), which have different spins at
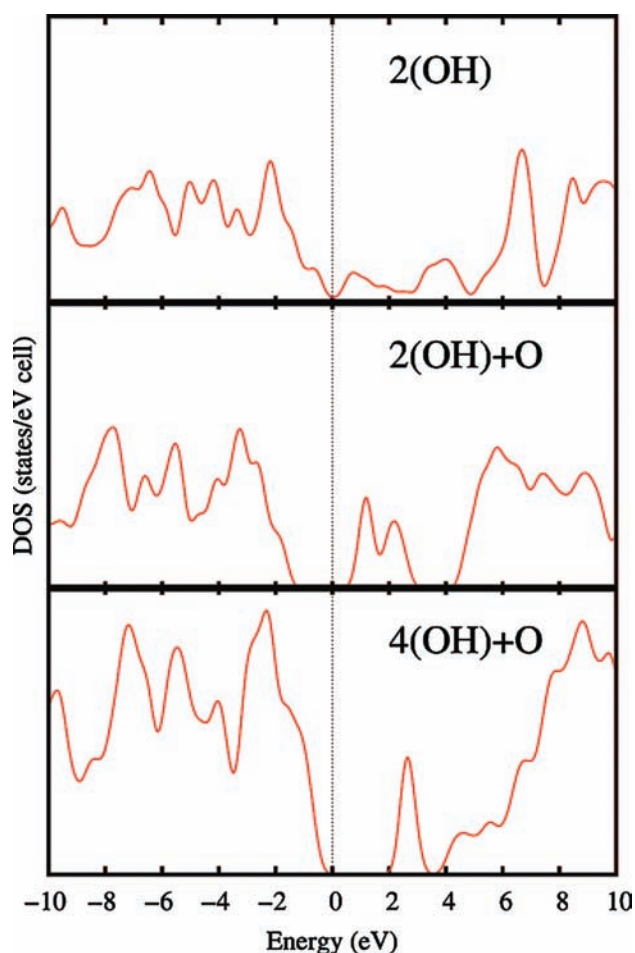

Fig. 16. Calculated electronic density of states for the most stable configurations at various degrees of coverage. Reprinted with permission from [54], D. W. Boukhvalov and M. I. Katsnelson, *J. Am. Chem. Soc.* 130, 10697 (**2008**). © (2008), American Chemical Society.
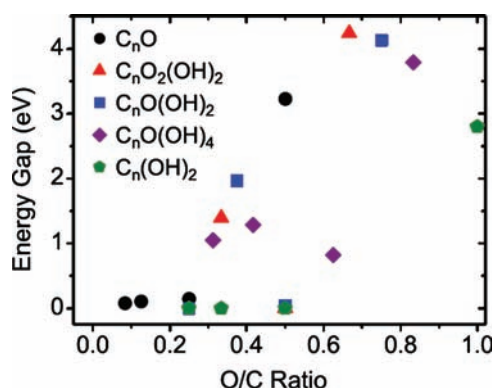

Fig. 17. Calculated energy gaps with respect to the overall oxygen-to-carbon ratio for different phases of graphene oxides. Reprinted with permission from [55], J.-A. Yan et al., *Phys. Rev. Lett.* 103, 086802 (**2009**). © (2009), American Physical Society.

ground states. Among them, the triplet **3d** has the lowest energy. The linear oxidations of **4** and **5** lead to the quintet **4c** and triplet **5b** as the lowest-energy isomers, respectively.

Several general conclusions can be drawn.
(1) When an all-benzenoid nanographene is linearly unzipped into oxygen-joined fragments, the oxidized benzenoid rings (aromatic sextets) selectively adopt the low-spin ($\Delta S = 0$) or high-spin conformation ($\Delta S = 1$) to yield the thermally most stable isomer. The selection of the conformation depends simply on the position of the aromatic sextets: the inner ones prefer the high-spin conformation, whereas the peripheral ones prefer the low-spin conformation. Therefore, the resulting most stable isomer has a total spin whose value equals the number of inner aromatic sextets (n_i) along the oxidizing line. The nanographene fragments contained in this isomer have a ferromagnetic spin coupling.
(2) Due to the tautomerization between the high-spin and low-spin conformations, there also exist other possible isomers with higher energies and with spins at ground state ranging from 0 to ($n_i - 1$). For example, in Figure 19, linear oxidations along *a1–a2*, *b1–b2*, and *c1–c2* will lead to ground-state oxides with $S = 2$, 1, and 2, respectively, and these oxides will isomerize to give at least ($n_i - 1$) higher-energy isomers with $S = 0$ through ($n_i - 1$), respectively.

6. REDUCTION MECHANISM OF GRAPHENE OXIDE

As summarized above, it is well accepted that four oxygen-containing groups exist in graphene oxide—epoxide, hydroxyl, carbonyl and carboxyl, and the later two are mainly located at graphene edges. Accordingly, Gao et al.[57] classified the oxygen functionalities into six categories: **A**, **A'**, **B**, **B'**, **C** and **D** (for the definitions, see Fig. 20).
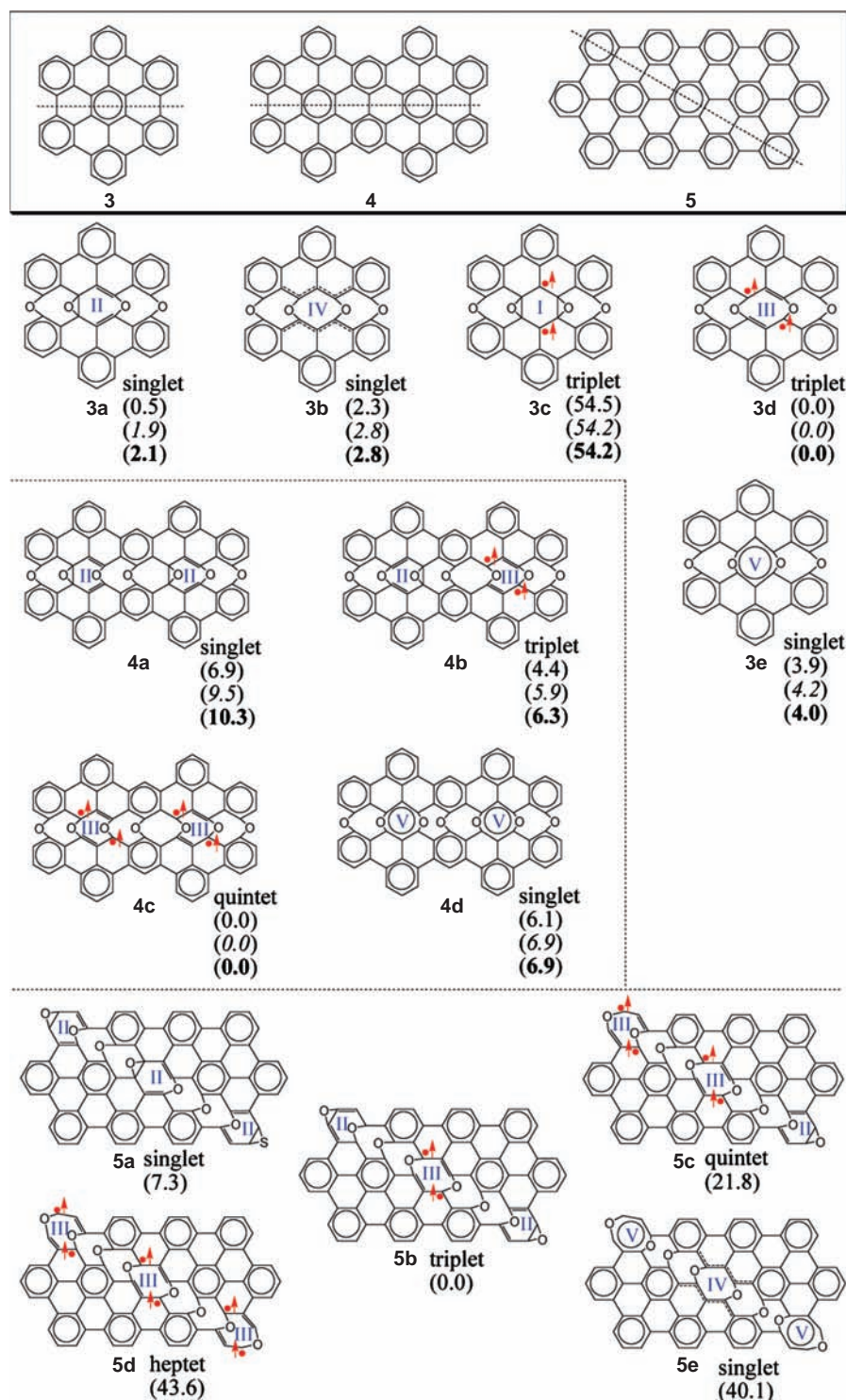
Fig. 18. All-benzenoid nanographenes and the oxides. Spin multiplicities are given; relative energies (E_{rel}, regular print), ZPE-corrected E_{rel} (italic print) and relative Gibb's free energies at 298.15 K (G_{rel}, bold print) at the (U)B3LYP/6-31G(d) level of theory are given in parentheses. The unit for energies is kcal/mol. The dashed lines (oxidizing lines) of nanographenes show the directions along which they are oxidized. Reprinted with permission from [56], X. Gao et al., *J. Am. Chem. Soc.* 131, 9663 (**2009**). © (2009), American Physical Society.

Using the DFT method (M05-2X/6-31G(d)) and series of cluster models, Gao et al. investigated reaction mechanisms for reducing these functionalities by hydrazine or heat treatment.[57] Three reaction mechanisms—*Routes 1,*

2 and *3*—were identified for reducing epoxide groups of graphene oxide using hydrazine as a reducing agent (Fig. 21). Their computations showed that *Routes 2* and *3* are dominant mechanisms when the epoxides are attached
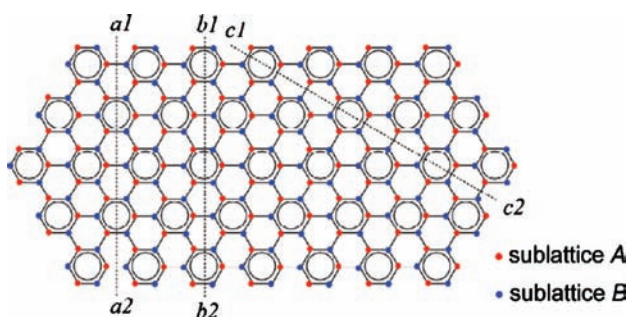
14

Fig. 19. Oxidation-unzipping of nanographene along dashed lines *a1–a2*, *b1–a2* and *c1–c2*. Reprinted with permission from [56], X. Gao et al., *J. Am. Chem. Soc.* 131, 9663 (**2009**). © (2009), American Physical Society.

to the aromatic domain, while *Route 1* is the exclusive mechanism when the epoxides protrude from graphene oxide. No reaction path was determined for reductions of hydroxyl, carbonyl, or carboxyl groups of graphene oxide using hydrazine as a reducing agent. The hydroxyl and carboxyl groups from graphene oxide can be eliminated by a high-temperature thermal annealing, which follow *Routes 5* and *7*, respectively. Kim et al.[58] independently studied hydrazine deepoxidation of graphene oxide, and obtained similar deepoxidation mechanisms.

When the epoxide groups are attached to the interior of an aromatic domain of graphene oxide, the hydrazine reductions are thermodynamically spontaneous with Gibbs free-energy barriers <48.3 kcal/mol at room temperature; in contrast, when an epoxide is located at the edges of an aromatic domain, the hydrazine reduction of an epoxide is blocked by the formation of a hydrazino alcohol via the first step in *Route 2*.

In comparison with the corresponding de-epoxidation products, the hydrazino alcohols are thermodynamically
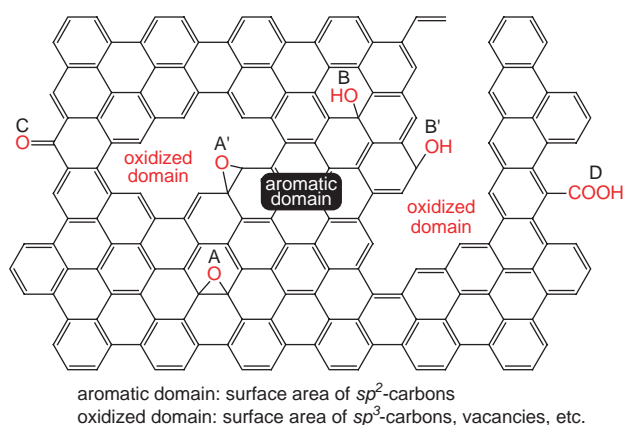

aromatic domain: surface area of sp^2-carbons
oxidized domain: surface area of sp^3-carbons, vacancies, etc.

Fig. 20. Schematic illustration of oxygen-containing groups in GO: **A**, epoxide located at the interior of an aromatic domain of GO; **A'**, epoxide located at the edge of an aromatic domain; **B**, hydroxyl located at the interior of an aromatic domain; **B'**, hydroxyl at the edge of an aromatic domain; **C**, carboxyl at the edge of an aromatic domain; and **D**, carboxyl at the edge of an aromatic domain.

more stable at room temperature. The thermal reductions of hydroxyls attached to the interior of an aromatic domain are also easier than those at the edges of the aromatic domain, similar to the case for de-exoxide reaction.

The Gibbs free-energy barrier of the hydrazine de-eposidations increases with increasing reaction temperature; thus higher temperature does not facilitate hydrazine de-epoxidation. However, an increased temperature is advantageous for the thermal de-hydroxylation of graphene oxide. These results infer that hydroxyl groups, including those at the edges of aromatic domains, can be eliminated from graphene oxide at temperatures higher than approximately 700 °C.

By analyzing the composition of residual oxygen-groups in chemically converted graphene, Gao et al. proposed new reaction procedures that may achieve an improved reduction efficiency (Fig. 22):[57] (i) treating GO with PPh$_3$/MOT at 55 °C in toluene to remove the epoxy groups and (ii) thermal annealing at temperatures >700 °C to eliminate the hydroxyls and carboxyls.

7. PERSPECTIVES

Graphite oxide, graphene oxide and chemically converted graphene are amorphous materials, which contain miscellaneous chemical groups and substructures. To a large extent, their chemical components and accurate structures still remain unclear. Therefore, the macroscopically observed chemistry of these materials is actually an overlap of diverse chemical processes. On the other hand, high-level applications of these materials require accurately addressing the structures and the associated physical and chemical properties. Persistent efforts in both experiment and theory towards the solutions are thus desired.

Chemical reactions, which have demonstrated their power in the high-yield and cheap synthesis of graphene from graphite, provide a valuable approach to engineer the structures and properties of graphenic materials. For this goal, a precise understanding of the mechanisms of the reactions occurring on graphite, graphene and their derivatives is essential. However, little progress has been achieved answering the mechanistic problems of graphene-related reactions. Many questions remain uncertain in this area. An intensive effort to study the reaction mechanisms, improve the reaction efficiency and design new purpose-oriented reactions is challenging but highly rewarding.

Though with many unsolved problems and challenges, these graphene-related materials are bringing us a new material revolution, and we can foreseen large-scale applications in the next decade or even sooner. Theoretical insights provided by the modern computational materials sciences combined with the continuous efforts from the experimental peers surely will help solve many perplexing problems in front of us, and further facilitate the process for us to fully achieve the potentials of these amazing materials.
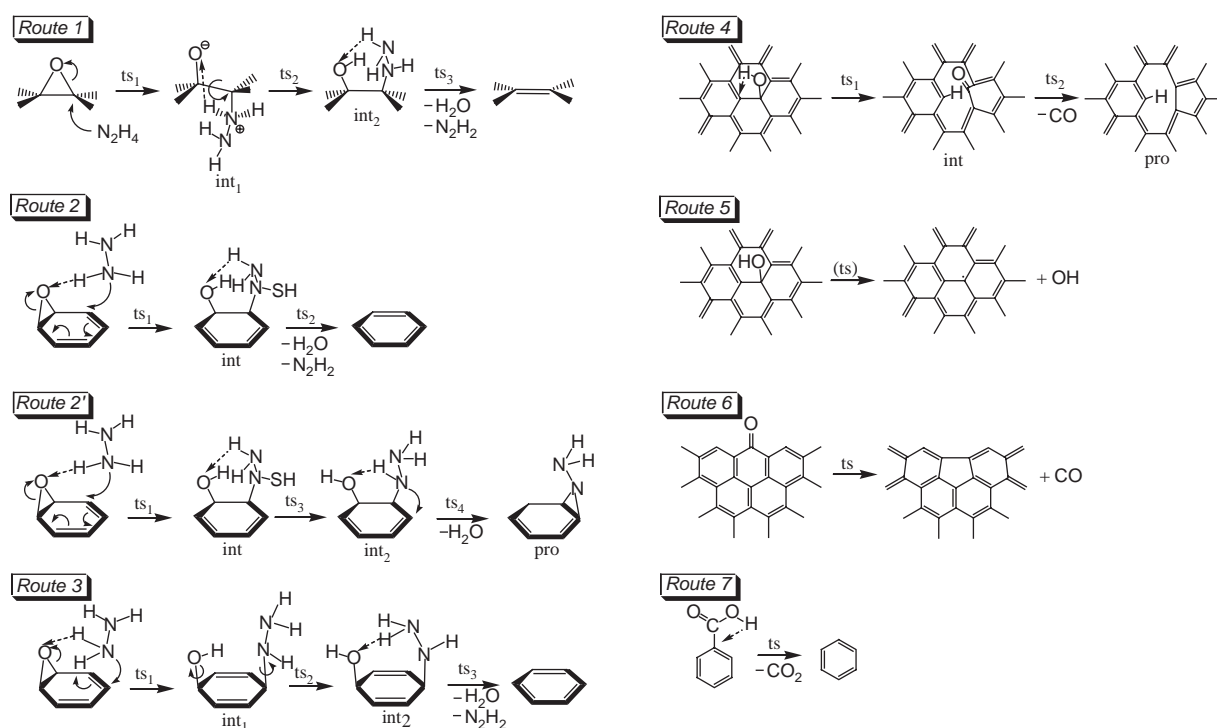
Fig. 21. Reduction mechanisms for graphene oxides. Routes 1-3 and 2' represent the mechanisms for the hydrazine de-epoxidation of graphene oxide. Routes 4 and 5 refer to the mechanism for the thermal de-hydroxylation of graphene oxide. Routes 6 and 7 respectively show the mechanisms for thermal de-carbonylation and thermal de-carboxylation of graphene oxide. Reprinted with permission from [57], X. Gao et al., *J. Phys. Chem. C* 114, 832 (**2010**). © (2010), American Physical Society.
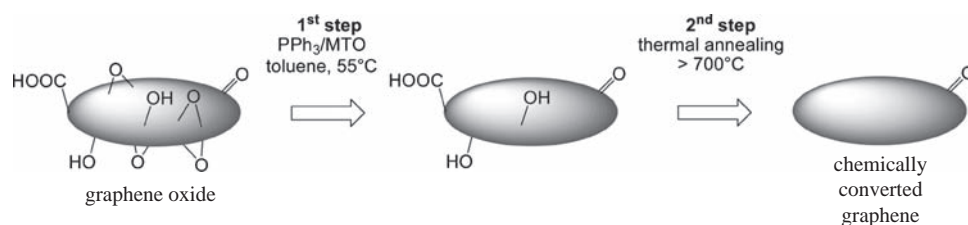

Fig. 22. A two-step chemical reduction proposed for the synthesis of chemically converted graphene from graphene oxide. Reprinted Figure 10 with permission from [57], X. Gao et al., *J. Phys. Chem. C* 114, 832 (**2010**). © (2010), American Physical Society.

References

1. P. R. Wallace, *Phys. Rev. Lett.* 71, 622 (**1947**).
2. K. S. Novoselov, A. K. Geim, S. V. Morozov, D. Jiang, Y. Zhang, S. V. Dubonos, I. V. Grigorieva, and A. A. Firsov, *Science* 306, 666 (**2004**).
3. S. Park and R. S. Ruoff, *Nat. Nanotechnol.* 4, 217 (**2009**).
4. M. J. Allen, V. C. Tung, and R. B. Kaner, *Chem. Rev.* 110, 132 (**2010**).
5. K. Müllen and J. P. Rabe, *Acc. Chem. Res.* 41, 511 (**2008**).
6. D. R. Dreyer, S. Park, C. W. Bielawski, and R. S. Ruoff, *Chem. Soc. Rev.* 39, 228 (**2010**).
7. K. P. Loh, Q. Bao, P. K. Ang, and J. Yang, *Chem. Soc. Rev.* 20, 2277 (**2010**).
8. O. C. Compton and S. T. Nguyen, *Small* 6, 711 (**2010**).
9. A. K. Geim and K. S. Novoselov, *Nat. Mater.* 6, 183 (**2007**).
10. A. K. Geim, *Science* 324, 1530 (**2009**).
11. J. Sakamoto, J. van Heijst, O. Lukin, A. D. Schlüter, *Angew. Chem. Int. Ed.* 48, 1030 (**2009**).
12. B. C. Brodie, *Philos. Trans. R. Soc. London* 149, 249 (**1859**).
13. L. Staudenmaier, *Ber. Dtsch. Chem. Ges.* 31, 1481 (**1898**).
14. W. S. Hummers and J. R. E. Offeman, *J. Am. Chem. Soc.* 80, 1339 (**1958**).
15. N. I. Kovtyukhova, P. J. Ollivier, B. R. Martin, T. E. Mallouk, S. A. Chizhik, E. V. Buzaneva, and A. D. Gorchinskiy, *Chem. Mater.* 11, 771 (**1999**).
16. M. Hirata, T. Gotou, S. Horiuchi, M. Fujiwara, and M. Ohba, *Carbon* 42, 2929 (**2004**).
17. M. Mermoux and Y. Chabre, *Synthetic Met.* 34, 157 (**1989**).

18. T. Szabó, O. Berkesi, P. Forgo, K. Josepovits, Y. Sanakis, D. Petridis, and I. Dékány, *Chem. Mater.* 18, 2740 (**2006**).
19. M. Mermoux, Y. Chabre, and A. Rousseau, *Carbon*, 469 (**1991**).
20. S. Stankovich, D. A. Dikin, R. D. Piner, K. A. Kohlhaas, A. Kleinhammes, Y. Jia, Y. Wu, S. T. Nguyen, and R. S. Ruoff, *Carbon* 45, 1558 (**2007**).
21. A. B. Bourlinos, D. Gournis, D. Petridis, T. Szabo, A. Szeri, and I. Dekany, *Langmuir* 19, 6050 (**2003**).
22. M. Hirata, T. Gotou, and M. Ohba, *Carbon* 43, 503 (**2005**).
23. S. Stankovich, R. D. Piner, X. Chen, N. Wu, S. T. Nguyen, and R. S. Ruoff, *J. Mater. Chem.* 16, 155 (**2006**).
24. S. Stankovich, R. D. Piner, S. T. Nguyen, and R. S. Ruoff, *Carbon* 44, 3342 (**2006**).
25. D. Cai and M. Song, *J. Mater. Chem.* 17, 3678 (**2007**).
26. D. A. Dikin, S. Stankovich, E. J. Zimney, R. D. Piner, G. H. B. Dommett, G. Evmenenko, S. T. Nguyen, and R. S. Ruoff, *Nature* 448, 457 (**2007**).
27. S. Gilje, S. Han, M. Wang, K. L. Wang, and R. B. Kaner, *Nano Lett.* 7, 3394 (**2007**).
28. N. A. Kotov, I. Dékány, and J. H. Fendler, *Adv. Mater.* 8, 637 (**1996**).
29. C. Gomez-Navarro, R. T. Weitz, A. M. Bittner, M. Scolari, A. Mews, M. Burghard, and K. Kern, *Nano Lett.* 7, 3499 (**2007**).
30. X. Fan, W. Peng, Y. Li, X. Li, S. Wang, G. Zhang, and F. Zhang, *Adv. Mater.* 20, 1 (**2008**).
31. G. Williams, B. Seger, and P. V. Kamat, *ACS Nano* 2, 1487 (**2008**).
32. M. J. McAllister, J.-L. Li, D. H. Adamson, H. C. Schniepp, A. A. Abdala, J. Liu, M. Herrera-Alonso, D. L. Milius, R. Car, R. K. Prud'homme, and I. A. Aksay, *Chem. Mater.* 19, 4396 (**2007**).
33. I. Jung, M. Pelton, R. Piner, D. A. Dikin, S. Stankovich, S. Watcharotone, M. Hausner, and R. S. Ruoff, *Nano Lett.* 7, 3569 (**2007**).
34. H. A. Becerril, J. Mao, Z. Liu, R. M. Stoltenberg, Z. Bao, and Y. Chen, *ACS Nano* 2, 463 (**2008**).
35. D. Yang, A. Velamakanni, G. Bozoklu, S. Park, M. Stoller, R. D. Piner, S. Stankovich, I. F. Jung, D A, C. A. Ventrice, Jr., and R. S. Ruoff, *Carbon* 47, 145 (**2009**).
36. K. Sendt and B. S. Haynes, *Proc. Combust. Inst.* 30, 2141 (**2004**).
37. K. Sendt and B. S. Haynes, *J. Phys. Chem. C* 111, 5465 (**2007**).
38. Z. H. Zhu, J. Finnerty, G. Q. Lu, and R. T. Yang, *Energy Fuels* 16, 1359 (**2002**).
39. J. M. Carlsson, F. Hanke, S. Linic, and M. Scheffler, *Phys. Rev. Lett.* 102, 166104 (**2009**).
40. S.-P. Chan, G. Chen, X. G. Gong, and Z.-F. Liu, *Phys. Rev. Lett.* 90, 086403 (**2003**).
41. D. Lamoen and B. N. J. Persson, *J. Chem. Phys.* 108, 3332 (**1998**).
42. F. Stevens, L. A. Kolodny, and T. P. Beebe, *J. Phys. Chem. B* 102, 10799 (**1998**).
43. J. M. Carlsson and M. Scheffler, *Phys. Rev. Lett.* 96, 046806 (**2006**).
44. J.-L. Li, K. N. Kudin, M. J. McAllister, R. K. Prud'homme, I. A. Aksay, and R. Car, *Phys. Rev. Lett.* 96, 176101 (**2006**).
45. J. T. Paci, T. Belytschko, and G. C. Schatz, *J. Phys. Chem. C* 111, 18099 (**2007**).
46. Z. Li, W. Zhang, Y. Luo, J. Yang, and J. G. Hou, *J. Am. Chem. Soc.* 131, 6320 (**2009**).
47. W. Cai, R. D. Piner, F. J. Stadermann, S. Park, M. A. Shaibat, Y. Ishii, D. Yang, A. Velamakanni, S. J. An, M. Stoller, J. An, D. Chen, and R. S. Ruoff, *Science* 321, 1815 (**2008**).
48. U. Hoffman and R. Holst, *Ber. Dtsch. Chem. Ges.* 72, 754 (**1939**).
49. G. Ruess, *Monatsch. Chem.* 76, 381 (**1946**).
50. W. Scholz and H.-P. Boehm, *Z. Anorg. Allg. Chem.* 369, 327 (**1969**).
51. T. Nakajima, A. Mabuchi, and R. Hagiwara, *Carbon* 26, 357 (**1988**).
52. T. Nakajima and Y. Matsuo, *Carbon* 32, 469 (**1994**).
53. L. B. Casabianca, M. A. Shaibat, W. W. Cai, S. Park, R. Piner, R. S. Ruoff, and Y. Ishii, *J. Am. Chem. Soc.* ASAP, doi: 10.1021/ja9030243.
54. D. W. Boukhvalov and M. I. Katsnelson, *J. Am. Chem. Soc.* 130, 10697 (**2008**).
55. J.-A. Yan, L. Xian, and M. Y. Chou, *Phys. Rev. Lett.* 103, 086802 (**2009**).
56. X. Gao, L. Wang, Y. Ohtsuka, D.-E. Jiang, Y. Zhao, S. Nagase, and Z. Chen, *J. Am. Chem. Soc.* 131, 9663 (**2009**).
57. X. Gao, J. Jang, and S. Nagase, *J. Phys. Chem. C* 114, 832 (**2009**).
58. M. C. Kim, G. S. Hwang, and R. S. Ruoff, *J. Chem. Phys.* 131, 064704 (**2009**).

REVIEW

J. Comput. Theor. Nanosci. 8, 1–17, **2011**

17